Schwinger boson mean field theories of spin liquid states on a honeycomb lattice: Projective symmetry group analysis and critical field theory

Fa Wang
Department of Physics, Massachusetts Institute of Technology, Cambridge, Massachusetts 02139, USA
(Received 18 May 2010; published 16 July 2010)

Motivated by the recent numerical evidence [Z. Meng, T. Lang, S. Wessel, F. Assaad, and A. Muramatsu, Nature (London) **464**, 847 (2010)] of a short-range resonating valence bond state in the honeycomb lattice Hubbard model, we consider Schwinger boson mean field theories of possible spin liquid states on honeycomb lattice. From general stability considerations the possible spin liquids will have gapped spinons coupled to Z_2 gauge field. We apply the projective symmetry group method to classify possible Z_2 spin liquid states within this formalism on honeycomb lattice. It is found that there are only two relevant Z_2 states, differed by the value of gauge flux, zero or π, in the elementary hexagon. The zero-flux state is a promising candidate for the observed spin liquid and continuous phase transition into commensurate Néel order. We also derive the critical field theory for this transition, which is the well-studied O(4) invariant theory [A. V. Chubukov, T. Senthil, and S. Sachdev, Phys. Rev. Lett. **72**, 2089 (1994); A. V. Chubukov, S. Sachdev, and T. Senthil, Nucl. Phys. B **426**, 601 (1994); S. V. Isakov, T. Senthil, and Y. B. Kim, Phys. Rev. B **72**, 174417 (2005)], and has an irrelevant coupling between Higgs and boson fields with cubic power of spatial derivatives as required by lattice symmetry. This is in sharp contrast to the conventional theory [S. Sachdev and N. Read, Int. J. Mod. Phys. B **5**, 219 (1991)], where such transition generically leads to incommensurate magnetic order. In this scenario the Z_2 spin liquid could be close to a tricritical point. Soft boson modes will exist at seven different wave vectors. This will show up as low-frequency dynamical spin susceptibility peaks not only at the Γ point (the Néel order wave vector) but also at Brillouin-zone-edge center M points and twelve other points. Some simple properties of the π-flux state are studied as well. Symmetry allowed further neighbor mean field ansatz are derived in appendices which can be used in future theoretical works along this direction.

DOI: 10.1103/PhysRevB.82.024419 PACS number(s): 75.10.Kt, 75.10.Jm

I. INTRODUCTION

Quantum ground state of a spin system without any spontaneous symmetry breaking, the so-called spin liquid, in two or higher spatial dimensions, has been a subject of intense research since it was first proposed more than thirty years ago.[1,2] These states, sometimes called resonating valence bond (RVB) states, generically appear in two varieties, the "short-range RVB state" with a gap to spin-carrying excitations, and the "critical spin liquid" with gapless spin excitations. Recently several candidate materials[3–5] have emerged for spin liquids in two spatial dimensions (2D). Interestingly they all have gapless spin excitations. Many parent Hamiltonians have also been constructed for spin liquids in 2D.[6–9] However, it remains unclear theoretically whether a simple and natural spin Hamiltonian, e.g., the Heisenberg model, can have a spin liquid ground state on some 2D lattices. For common bipartite 2D lattices, the square and honeycomb lattices, quantum Monte Carlo (QMC) (Refs. 10 and 11) and other calculations[12–18] have clearly shown the long-range magnetic order in the ground state of the nearest-neighbor Heisenberg model. Therefore frustration is usually considered as an important ingredient for stabilizing the putative spin liquid states.

In an exciting paper by Meng *et al.*,[19] the half-filled Hubbard model on honeycomb lattice Eq. (1) was carefully studied by quantum Monte Carlo calculations. The model simply consists of hopping of electrons on nearest-neighbor bonds $\langle ij\rangle$ and onsite repulsion between two spin species labeled by $\alpha=\uparrow,\downarrow$

$$H=-t\sum_{\langle ij\rangle,\alpha}(c_{i\alpha}^{\dagger}c_{j\alpha}+c_{j\alpha}^{\dagger}c_{i\alpha})+U\sum_{i}n_{i\uparrow}n_{j\downarrow}. \quad (1)$$

Varying the only parameter in the problem, the ratio of onsite repulsion $U>0$ and electron hopping t, three different phases were observed. With small coupling $U/t<3.5$ the system is a semimetal with Dirac-type dispersion. For large coupling $4.3<U/t$ the system develops long-range magnetic order. In the intermediate coupling region $3.5<U/t<4.3$ a very interesting state with both single-particle gap and spin gap appears. Various symmetry-breaking scenarios were checked in this state and then ruled out. It was thus concluded that this state is a genuine short-range RVB state.

This is somewhat surprising considering both weak- and strong-coupling limits. Starting from the weak-coupling limit, with the single-particle gap develops continuously as observed in the calculation,[19] it was expected that the spin dynamic will either inherit the gapless nature of the small U semimetal phase,[20] or develop certain kind of spontaneous symmetry breaking.

In the strong-coupling large $U\rightarrow+\infty$ limit the low-energy Hamiltonian is the nearest-neighbor spin-1/2 Heisenberg antiferromagnetic (AFM) model whose ground state has long-range colinear Néel order[11] and must have gapless spin-wave excitations as Goldstone modes. Indeed a magnetic order was seen in the strong-coupling region $4.3<U/t$ in the numerical simulation.[19] Moreover the magnetic-order parameter and spin gap seem to both vanish continuously at the critical point $U/t\approx4.3$. This raises the hope to understand

 ©2010 The American Physical Society

the observed short-range RVB state, at least in the large U/t part of the parameter range, by going from the strong-coupling side. Although the conventional wisdom[21,22] is that such continuous quantum phase transition between colinear magnetic order and gapped spin liquid is impossible.

In the strong-coupling regime, with single-particle gap much larger than the spin gap (zero in magnetic ordered phase), it is reasonable to describe the low-energy physics by an effective spin-1/2 Hamiltonian, which can be derived from the Hubbard model and should be[23] (up to t^4/U^3 order)

$$H_{\text{spin}} = \sum_{\langle ij\rangle} \left(\frac{4t^2}{U} - \frac{16t^4}{U^3} \right) \mathbf{S}_i \cdot \mathbf{S}_j + \sum_{\langle\langle ij\rangle\rangle} \frac{4t^4}{U^3} \mathbf{S}_i \cdot \mathbf{S}_j + \cdots, \quad (2)$$

where $\langle\langle ij\rangle\rangle$ are next-nearest-neighbor bonds. As the short-range RVB region is still close to the single-particle gap opening transition (Mott transition), the spin Hamiltonian should be much more complex than this leading-order Heisenberg model, i.e., have strong couplings of further neighbors and/or four and even more spins. Solving the exact spin model will likely not be easier than solving the original Hubbard model. In this paper we take a different approach. Using symmetry analysis we completely classify all possible stable gapped spin liquid states within the Schwinger boson formalism. It turns out that there are only two relevant states, differed by the gauge-invariant flux, zero or π, in a hexagon. Some signatures of these two spin liquid states will be derived which may be checked in numerical simulations. The zero-flux state turns out to be a very promising candidate for the observed short-range RVB state. We obtain a mean field "phase diagram" (Fig. 1) for it in terms of a variational parameter, which could qualitatively agree with the behavior of the Hubbard model close to the magnetic transition. Our symmetry analysis fixes symmetry allowed forms of further neighbor mean field couplings, which will be useful for later theoretical studies of spin liquids on honeycomb lattice.

The outline of this paper is as follows. In Sec. II we briefly describe the formalism of Schwinger boson mean field theory. In Sec. III we apply the projective symmetry group method developed in Ref. 24 to classify all Z_2 Schwinger boson states on honeycomb lattice. Details of the derivation are presented in Appendix A. Two out of 32 possible Z_2 states are particularly relevant here and we derive the mean field ansatz up to fourth neighbors in Appendix B. In Sec. IV we study some simple properties of the two Z_2 Schwinger boson states emerged from the projective symmetry group (PSG) analysis. And we derive the continuum-field theory for the transition from the zero-flux Z_2 spin liquid to the Néel order in Appendix C. Conclusions and outlook of further developments are summarized in Sec. V.

II. SCHWINGER BOSON MEAN FIELD THEORY FOR Z_2 SPIN LIQUIDS

A microscopic theory of spin liquid usually involves fractionalized spin-carrying particles, the spinons, which are strongly coupled to certain emergent-gauge field.[21,25–27] It is generally believed that, when the spinons are gapped, the system is stable only if the gauge field takes discrete values[22,26] (some exotic counter-examples exist such as the doubled Chern-Simons model of Levin and Wen[28] but will not be considered here). The natural candidate of such discrete gauge field for short-range RVB state is the Z_2 (Ising) gauge theory.[29] Thus throughout this paper we will assume a Z_2 spin liquid state on the honeycomb lattice without breaking of any physical symmetry.

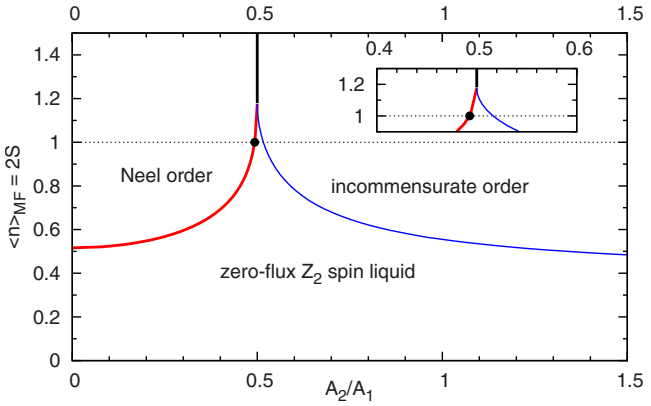

FIG. 1. (Color online) Mean field phase diagram of the zero-flux state. Horizontal axis is the variational parameter, ratio between next-nearest-neighbor and nearest-neighbor mean field couplings, A_2/A_1. Vertical axis is the average boson density $\langle \hat{n} \rangle_{\text{MF}}$. The dash line $\langle \hat{n} \rangle_{\text{MF}}=1$ indicates the boson density of spin-1/2 system. Solid lines are phase boundaries. The red solid line between the zero-flux Z_2 spin liquid and the Néel order is a continuous transition described by the field theory Eq. (22). The vertical solid black line between the two ordered states is a first-order transition. The blue line between the Z_2 spin liquid and the incommensurate magnetic order has yet to be studied but is likely a continuous transition. There is a very small parameter range of $0.493 < A_2/A_1 < 0.516$ (see also the inset) such that a spin-1/2 system will be a gapped Z_2 spin liquid, which is a promising explanation of the observed spin liquid (Ref. 19). The variational parameter A_2/A_1 can, in principle, be tuned by physical parameters. For example, as argued in Sec. IV, increase in U/t will decrease A_2/A_1, which can drive a continuous magnetic-ordering transition at the crossing point (black dot) of the dash line and the red solid line.

There are several serious problems of the Z_2 spin liquid assumption in the context of the QMC result.[19] First if the magnetic-ordered phase is continuously connected to a Z_2 spin liquid, it will usually be noncollinear and incommensurate,[21] unlike the observed commensurate Néel-type order. However, it will be seen later in this paper that this expectation is not correct on honeycomb lattice. Also it seems that the possibility of noncollinear magnetic order has not been carefully checked in the paper by Meng *et al.*[19] Thus we believe this argument against a Z_2 spin liquid explanation may be circumvented. The second problem is the claim made by Meng *et al.*[19] that topological degeneracy was not observed while a Z_2 spin liquid on a torus should have fourfold-degenerate ground states. But it was acknowledged that their numerical method might have missed the degenerate ground states in other topological sectors. Despite this uncertainty we believe that it is still meaningful to thoroughly study the possibilities of Z_2 spin liquids on honeycomb lattice.

Another issue for the Schwinger boson formalism is that it is not convenient for the description of the seemingly continuous Mott transition around $U/t \approx 3.5$ in the numerical results.[19] We will refrain from considering that parameter range in this paper and strictly limit ourselves in the strong-coupling region with large single-particle gap.

To continuously evolve from a magnetic ordered state to a Z_2 spin liquid with spin gap, a natural approach is to decompose each spin into two bosonic spinons, the Schwinger bosons.[21,25,26] The magnetic-ordering transition then becomes the condensation of these bosons.[21,25,26,30] And a large-N Sp(N) generalization has been formulated to study the problem in a controlled $1/N$ expansion.[21,25,26] It is also possible to get a gapped Z_2 spin liquid from fermionic spinons[27] but that scenario will not be considered in this paper. In this paper we will not use the Sp(N) language but the PSG analysis can be directly applied to the large-N theory.

In the following we briefly recall the formulation of the Schwinger boson mean field theory. More details can be found in, for example, Ref. 30.

The bosonic representation of spin $\mathbf{S}_i$ on site i is

$$\mathbf{S}_i = \frac{1}{2}\sum_{\alpha,\beta} b_{i\alpha}^{\dagger}\boldsymbol{\sigma}_{\alpha\beta}b_{i\beta} \tag{3}$$

with boson operators b, spin indices $\alpha,\beta=\uparrow,\downarrow$, and Pauli matrices $\boldsymbol{\sigma}$. For this to be a faithful representation of the spin system a constraint on the total boson number must be imposed

$$\hat{n}_i \equiv \sum_{\alpha} b_{i\alpha}^{\dagger}b_{i\alpha} = 2S, \tag{4}$$

where S is the size of the spin. For spin-1/2 model, $S=1/2$, the boson density should be unity. This hard constraint will be relaxed in the mean field treatment so it is only satisfied on average under the mean field state

$$\langle \hat{n}_i \rangle_{\mathrm{MF}} = \kappa, \tag{5}$$

where $\langle\cdot\rangle_{\mathrm{MF}}$ means expectation value in the mean field theory, and the average boson density κ can also be taken as a parameter.[30]

Possible mean field decouplings of Heisenberg interaction $\mathbf{S}_i\cdot\mathbf{S}_j$ can be suggested from the operator identities ($i\neq j$)

$$\begin{aligned}\mathbf{S}_i\cdot\mathbf{S}_j &= -2\hat{A}_{ij}^{\dagger}\hat{A}_{ij} + (1/4)\hat{n}_i\hat{n}_j \\ &= -(1/4)\hat{n}_i\hat{n}_j + 2\hat{B}_{ij}^{\dagger}\hat{B}_{ij} = \hat{B}_{ij}^{\dagger}\hat{B}_{ij} - \hat{A}_{ij}^{\dagger}\hat{A}_{ij},\end{aligned} \tag{6}$$

where $\hat{A}_{ij}=(1/2)(b_{i\uparrow}b_{j\downarrow}-b_{i\downarrow}b_{j\uparrow})$ and $\hat{B}_{ij}=(1/2)(b_{i\uparrow}^{\dagger}b_{j\uparrow}+b_{i\downarrow}^{\dagger}b_{j\downarrow})$ are both SU(2) invariant.

A mean field theory for Heisenberg AFM model will generally include both $\hat{A}$ and $\hat{B}$ terms[31–33]

$$\begin{aligned}H_{\mathrm{MF}} = &\sum_{i,j}(A_{ij}^{*}\hat{A}_{ij} - B_{ij}^{*}\hat{B}_{ij} + \mathrm{H.c.}) + \sum_{i}\mu_i(\hat{n}_i-\kappa) \\ &+ \sum_{i,j}(A_{ij}^{*}A_{ij} - B_{ij}^{*}B_{ij})/J_{ij},\end{aligned} \tag{7}$$

where $A_{ij}=-A_{ji}$, $B_{ij}=B_{ji}^{*}$ are complex numbers called the mean field ansatz and the chemical potential μ_i is introduced to achieve the average constraint Eq. (5). For translationally invariant states $\mu_i=\mu$ are uniform. And $A_{ij}(B_{ij})$ on symmetry related bonds will have the same magnitude. Both A and B terms have been consistently generalized to the theory of Sp(N) magnets and the mean field Hamiltonian can be regarded as a saddle-point solution of the Sp(N) action after Hubbard-Stratonovich transformation.[34] Here we will not use the Sp(N) language and we will regard the mean field theory as a variational approach for general spin models even beyond Heisenberg model.

The mean field Hamiltonian can be diagonalized to solve for boson dispersions. For small boson density κ the bosons will be gapped. Increasing boson density will cause boson condensation at a critical boson density κ_c, which corresponds to a magnetic-ordering transition and the details of the magnetic order can be derived from the structure of the boson condensates.[30]

For the Heisenberg model, the mean field ansatz can be solved from the self-consistent equations

$$\langle\hat{A}_{ij}\rangle_{\mathrm{MF}} = -A_{ij}/J_{ij}, \quad \langle\hat{B}_{ij}\rangle_{\mathrm{MF}} = -B_{ij}/J_{ij} \tag{8}$$

together with the average constraint Eq. (5). Self-consistent equations for non-Heisenberg models can, in principle, be derived as well.

As discussed in Ref. 24, for the emergent-gauge theory to be Z_2, it will need either both ansatz A_{ij} and B_{ij}, or only ansatz A_{ij} but with geometric frustration. Nearest-neighbor ansatz $A_{\langle ij\rangle}$ on honeycomb lattice is bipartite and will lead to a U(1) gauge theory. Since the spin Hamiltonian Eq. (2) have strong further neighbor couplings, it is natural to assume that next-nearest-neighbor $A_{\langle\langle ij\rangle\rangle}$ is nonzero, which is sufficient to "Higgs" the U(1) gauge field into Z_2.

III. PROJECTIVE SYMMETRY GROUP OF SCHWINGER BOSON MEAN FIELD THEORIES ON HONEYCOMB LATTICE

The mean field theory Eq. (7) is not invariant under the local U(1) gauge transformations of the Schwinger bosons

$$b_{j\alpha} \to e^{i\phi(i)}b_{j\alpha}, \quad \alpha=\uparrow,\downarrow, \tag{9}$$

where the phase $\phi(j)$ can depend on site j. The ansatz will transform accordingly as

$$A_{ij} \to e^{i[\phi(i)+\phi(j)]}A_{ij}, \quad B_{ij} \to e^{i[-\phi(i)+\phi(j)]}B_{ij}. \tag{10}$$

However, the physical spin state is gauge invariant if the constraint Eq. (4) is implemented exactly. Thus different mean field ansatz may correspond to the same physical state. Moreover the physical symmetries, e.g., the space-group symmetry may not be explicitly present in the mean field ansatz. And it is not straightforward to test whether a given mean field ansatz actually conforms all the physical symmetries under the constraint Eq. (4). It was first noted by Wen and collaborators, in the studies of fermionic mean field theories of spin liquids, that the mean field theory should have a projective symmetry.[35,36] Namely, the mean field ansatz should be invariant under a combined physical symme-

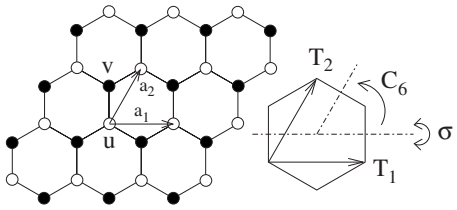

FIG. 2. The honeycomb lattice is shown on the left. Open (filled) circles indicate the two sublattices. $\mathbf{a}_1,\mathbf{a}_2$ are primitive vectors. For simplicity we assume the lattice constant $a=|\mathbf{a}_1|=|\mathbf{a}_2|=1$. u,v denote the two sites within one unit cell. The hexagon on the right is the enlarged unit cell with schematic illustration of the space-group generators, translations T_1 and T_2, sixfold rotation C_6, and reflection σ.

try group and gauge-group operation, a projective symmetry group operation. The structure of the physical symmetry group constrains possible structures of this projective symmetry group, thus constrains possible spin liquid states. This idea was generalized to Schwinger boson states in Ref. 24 and applied to triangular and kagome lattices. Here we will directly apply it to honeycomb lattice. More detailed discussion of the formalism can be found in Ref. 24.

The honeycomb lattice and its space-group generators are illustrated in Fig. 2. Sites are labeled as (x,y,w) with integer x,y indicating the unit cell at $x\mathbf{a}_1+y\mathbf{a}_2$, and $w=u,v$ indicates the two sites in the unit cell.

The space group of honeycomb lattice is generated by two translations T_1 along $\mathbf{a}_1$, and T_2 along $\mathbf{a}_2$, and a counterclockwise sixfold rotation C_6 around the hexagon center $(1/3)(\mathbf{a}_1+\mathbf{a}_2)$, and a reflection σ around the horizontal axis through the same hexagon center. Their actions on the lattice are

$$T_1:(x,y,w)\to(x+1,y,w),\quad w=u,v, \tag{11a}$$

$$T_2:(x,y,w)\to(x,y+1,w),\quad w=u,v, \tag{11b}$$

$$C_6:\begin{cases}(x,y,u)\to(-y+1,x+y-1,v)\\(x,y,v)\to(-y,x+y,u)\end{cases}, \tag{11c}$$

$$\sigma:\begin{cases}(x,y,u)\to(x+y,-y,v)\\(x,y,v)\to(x+y,-y,u)\end{cases}. \tag{11d}$$

We associate a U(1) gauge-group element, $e^{i\phi_X(j)}$ dependent on site j, to each element X of the space group, and demand that the mean field ansatz be invariant under the combined PSG operation

$$b_{j\alpha}\to e^{i\phi_X[X(j)]}b_{X(j)\alpha},\quad \alpha=\uparrow,\downarrow, \tag{12}$$

where $X(j)$ is the image of site j under the action of X. The structure of the space group can be used for solving the allowed phase functions $\phi_X(j)$. The solution is straightforward and listed in Appendix A. In the end we have

$$\phi_{T_1}(x,y,w)=0,\quad \phi_{T_2}(x,y,w)=p_1\pi x,$$

$$\phi_{C_6}(x,y,w)=p_1\pi\frac{x(x+2y-1)}{2}+\frac{(p_7+p_8+p_9)\pi}{2},$$

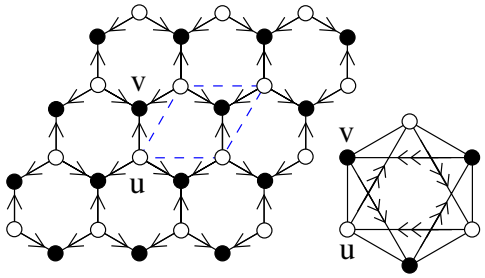

FIG. 3. (Color online) The zero-flux ansatz. Left part shows the nearest-neighbor ansatz. Single arrow from i to j means $A_{\langle ij\rangle}=-A_{\langle ji\rangle}=A_1>0$. All nearest-neighbor $B_{\langle ij\rangle}$ must be zero according to Appendix B. Blue dash rhombus is the unit cell of the mean field theory, containing two sites u,v. The large hexagon on the right is the enlarged mean field unit cell showing the next-nearest-neighbor bonds. Double arrow from i to j means $A_{\langle\langle ij\rangle\rangle}=-A_{\langle\langle ji\rangle\rangle}=A_2$. All next-nearest-neighbor $B_{\langle\langle ij\rangle\rangle}=+B_2$ are real according to Eqs. (B5a)–(B5f).

$$\phi_\sigma(x,y,u)=p_1\pi\left[\frac{y(y-1)}{2}+x\right]+p_5\pi y+\frac{(p_7+p_9)\pi}{2},$$

$$\phi_\sigma(x,y,v)=p_1\pi\left[\frac{y(y-1)}{2}+x\right]+p_5\pi y+\frac{(p_7-p_9)\pi}{2} \tag{13}$$

with $w=u,v$ labels sublattice, and five free integer parameters $p_1,p_5,p_7,p_8,p_9=0,1 \bmod 2$. Therefore there are at most 32 Z_2 states. Requiring nonzero nearest-neighbor $A_{\langle ij\rangle}$, which is natural for strong nearest-neighbor Heisenberg AFM coupling, eliminates three parameters, $p_5=p_1$, $p_7=1$, and $p_9=p_8$. If next-nearest-neighbor $A_{\langle\langle ij\rangle\rangle}$ is also nonzero as discussed in the end of Sec. II, one more parameter can be eliminated, $p_8=1$, and we are left with only one free parameter $p_1=0,1$. So there are only two relevant Z_2 states with

$$\phi_{T_1}(x,y,w)=0,\quad \phi_{T_2}(x,y,w)=p_1\pi x,$$

$$\phi_{C_6}(x,y,w)=p_1\pi\frac{x(x+2y-1)}{2}-\frac{\pi}{2},$$

$$\phi_\sigma(x,y,u)=p_1\pi\left[\frac{y(y-1)}{2}+x+y\right]+\pi,$$

$$\phi_\sigma(x,y,v)=p_1\pi\left[\frac{y(y-1)}{2}+x+y\right]. \tag{14}$$

From the solutions of PSG one can construct all symmetry-allowed mean field ansatz. The expressions of A_{ij} up to fourth neighbors and B_{ij} up to next-nearest neighbor are listed in Appendix B. The nearest-neighbor and next-nearest-neighbor A_{ij} are also illustrated in Figs. 3 and 4 for zero- and π-flux states, respectively. In this paper the magnitudes of nearest-neighbor $|A_{\langle ij\rangle}|$ and next-nearest-neighbor $|A_{\langle\langle ij\rangle\rangle}|$ are denoted as A_1 and A_2, respectively. The two states are more intuitively distinguished by the gauge-invariant flux[37] in the elementary hexagon, defined as the phase of $A_{ij}(-A^*_{jk})A_{k\ell}(-A^*_{\ell m})A_{mn}(-A^*_{ni})$, where the six sites

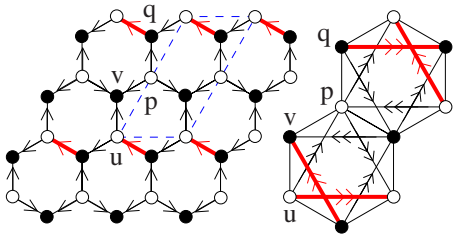

FIG. 4. (Color online) The π-flux ansatz. Left part shows the nearest-neighbor ansatz. Single arrow from i to j means $A_{\langle ij\rangle}=-A_{\langle ji\rangle}=A_1>0$. All nearest-neighbor $B_{\langle ij\rangle}$ must be zero according to Appendix B. Blue dash rhombus is the doubled unit cell of the mean field theory, containing four sites u,v,p,q. The large double hexagon on the right is the enlarged mean field unit cell showing the next-nearest-neighbor bonds. Double arrow from i to j means $A_{\langle\langle ij\rangle\rangle}=-A_{\langle\langle ji\rangle\rangle}=A_2$. All next-nearest-neighbor $B_{\langle\langle ij\rangle\rangle}=\pm B_2$ are real, with the $\pm$ signs given in Eqs. (B5a)–(B5f). Red thick bonds are those different from the zero-flux ansatz Fig. 3.

i,j,k,ℓ,m,n are around a hexagon. For these two states this flux is $p_1\pi$ so the time-reversal symmetry is also satisfied.

IV. Z_2 SPIN LIQUIDS ON HONEYCOMB LATTICE

In this section we study, within the mean field treatment, some simple properties of the two Z_2 spin liquid states found through the PSG analysis. For simplicity we will only use nearest-neighbor $A_{\langle ij\rangle}=\pm A_1$ and next-nearest-neighbor bonds $A_{\langle\langle ij\rangle\rangle}=\pm A_2$ with A_1 real positive. The $\pm$ signs are given in Figs. 3 and 4. Because the spin Hamiltonian is very complicated, we will not compute energetics of these states and will not derive/solve self-consistent equations of ansatz A_1,A_2. Instead we will treat the ratio A_2/A_1 as a variational parameter and study the phase diagram with respect to it. This parameter can, in principle, be tuned by, for example, the J_2/J_1 ratio in the nearest-neighbor next-nearest-neighbor J_1-J_2 Heisenberg AFM model on honeycomb lattice, which is proportional to $(t/U)^2$ for small t/U [see, e.g., Eq. (2)].

Note that the J_1-J_2 Heisenberg model on honeycomb lattice has been studied within a Schwinger boson formalism by Mattsson *et al.*[38] However, only the nearest-neighbor $A_{\langle ij\rangle}$ and next-nearest-neighbor $B_{\langle\langle ij\rangle\rangle}$ were used. So that theory has U(1) gauge field instead of Z_2 and will be unstable. More recently Cabra *et al.*[39] studied a J_1-J_2-J_3 model with $J_3=J_2$ using Schwinger boson mean field theory. They found a commensurate colinear magnetic order with large J_2/J_1, which is different from the incommensurate order obtained in the present paper with large A_2/A_1 in the zero-flux state, The small J_2/J_1 region of phase diagram in Ref. 39 qualitatively agrees with our small A_2/A_1 region for the zero-flux state in Fig. 1.

A. Zero-flux state

The zero-flux Z_2 spin liquid (Fig. 3) is a promising candidate for the numerically observed short-range RVB state. It has gapped bosonic spinons coupled to Z_2 gauge field. And it has a continuous transition into the Néel order even with small nonzero next-nearest-neighbor mean field coupling A_2, as long as $A_2<A_1/2$. The continuum-field theory close to this transition is derived following the method in Ref. 40. The effective theory shows a nontrivial coupling of bosons to the Higgs field involving cubic power of spatial derivatives, which allows a direct transition from Z_2 spin liquid to Néel order. This is in contrast to the conventional theory of transition between Z_2 spin liquid and magnetic-ordered state[21] which will generically give a noncollinear incommensurate magnetic order.

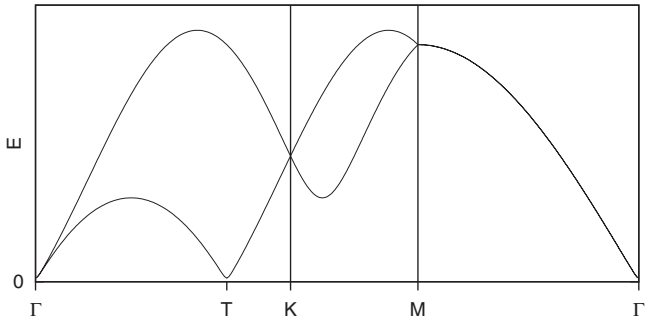

FIG. 5. The zero-flux mean field boson dispersion $E_\pm$ Eq. (19), with $A_2/A_1=1/2$ and average boson density $\langle\hat{n}\rangle_{\rm MF}=1$ (for spin-1/2 model), along high-symmetry directions Γ-K-M-Γ [see Fig. 6(a)]. Note the very low-energy boson modes at T point.

The unit cell of Fig. 3 contains two sites u,v. Fourier transform the bosons on each sublattice $(w=u,v)$

$$b_{(x,y,w)\alpha}=\frac{1}{\sqrt{N_{\rm unit\ cells}}}\sum_{\mathbf{k}} e^{-i(k_1x+k_2y)}b_{\mathbf{k}w\alpha}, \tag{15}$$

where $k_{1,2}\equiv\mathbf{k}\cdot\mathbf{a}_{1,2}$, the mean field Hamiltonian Eq. (7) becomes, up to a constant

$$H_{\rm MF}=\sum_{\mathbf{k}}\Psi_{\mathbf{k}}^\dagger\begin{pmatrix}\mu\mathbf{1}_{2\times2} & A_1P_1+A_2P_2\\ -A_1P_1-A_2^*P_2 & \mu\mathbf{1}_{2\times2}\end{pmatrix}\Psi_{\mathbf{k}}, \tag{16}$$

where $\Psi_{\mathbf{k}}$ is a four component field $\Psi_{\mathbf{k}}=(b_{\mathbf{k}u\uparrow},b_{\mathbf{k}v\uparrow},b^\dagger_{-\mathbf{k},u\downarrow},b^\dagger_{-\mathbf{k},v\downarrow})^T$ (superscript ^{T} means transpose), $\mathbf{1}_{2\times2}$ is 2×2 identity matrix, and $P_{1,2}(\mathbf{k})$ are 2×2 antihermitian matrices

$$P_1(\mathbf{k})=\begin{pmatrix}0 & \dfrac{+1+e^{i(k_1-k_2)}+e^{-ik_2}}{2}\\ \dfrac{-1-e^{i(k_2-k_1)}-e^{ik_2}}{2} & 0\end{pmatrix} \tag{17}$$

and

$$P_2(\mathbf{k})=i[\sin(k_2)-\sin(k_1)+\sin(k_1-k_2)]\mathbf{1}_{2\times2}. \tag{18}$$

The mean field Hamiltonian can be diagonalized by a Bogoliubov transformation.[30] The mean field dispersion has two branches $E_\pm$, each is doubly degenerate

$$E_\pm(\mathbf{k})=\sqrt{\mu^2-A_1^2f_1\mp2A_1\Re A_2\sqrt{f_1}f_2-|A_2|^2(f_2)^2}, \tag{19}$$

where $f_1=[3+2\cos(k_1)+2\cos(k_2)+2\cos(k_1-k_2)]/4$, $f_2=4\sin(k_1/2)\sin(k_2/2)\sin[(k_1-k_2)/2]$, and $\Re A_2$ is the real part of A_2. An example of the dispersion is shown in Fig. 5.

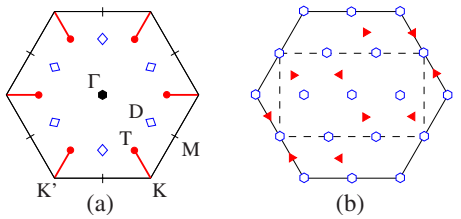

FIG. 6. (Color online) (a) Hexagon is the Brillouin zone of the zero-flux ansatz. Central black dot is the Γ point $(k_1,k_2)=(0,0)$, where boson condensation happens when $A_2/A_1<1/2$. When A_2/A_1 increases from 1/2 to $+\infty$, the boson condensation momenta move along the red short lines, $\pi<|\mathbf{k}|<4\pi/3$, from T to $K(K')$. The Γ point, three BZ edge center M points, six T points (filled red circle, $|\mathbf{k}|=\pi$) on Γ-$K(K')$ lines, and six D points (open blue diamond, $|\mathbf{k}|=\sqrt{3}\pi/2$) on Γ-$M$ lines are the would-be magnetic Bragg peaks for zero-flux spin liquid with $A_2/A_1\sim 1/2$, namely, peaks in dynamical spin susceptibility at low frequency around spin gap. (b) Hexagon is the Brillouin zone of the original lattice. Dash rectangle is the reduced Brillouin zone for the π-flux ansatz. In the π-flux state, bosons can condense at the momenta indicated by the filled red small triangles and produce magnetic Bragg peaks with possible wave vectors indicated by the open blue small hexagons.

When the dispersion is gapped, $E_{\pm}>0$, the average boson number $\kappa\equiv\langle\hat{n}\rangle_{\mathrm{MF}}$ is

$$\kappa=\int\frac{dk_1dk_2}{4\pi^2}\frac{1}{2}\left[\frac{|\mu|}{E_+(\mathbf{k})}+\frac{|\mu|}{E_-(\mathbf{k})}\right]-1. \tag{20}$$

Since we want the system to be stable against magnetic ordering, we want to maximize its capability of containing bosons. When A_1 and magnitude $|A_2|$ are fixed, the above boson density will be maximized if A_2 is real. Therefore A_2 will be assumed as real positive hereafter (real negative A_2 case is related to real positive case by a gauge transformation).

When $A_2<A_1/2$ the dispersion minimum is at the Γ point, $(k_1,k_2)=(0,0)$, in the Brillouin zone (BZ) [see Fig. 6(a)]. With increasing boson density the bosons will finally condense at the Γ point. Like in the triangular and kagome case,[24,30] the structure of the condensate can be determined by solving the eigenvectors of Eq. (16) with zero eigenvalues at the condensation momenta. Let $(k_1,k_2)=(0,0)$ in Eq. (16) and demand (one of) $E_{\pm}$ to be zero, we get $|\mu/A_1|=3/2$ and two eigenvectors $(1,0,0,-1)^T$, $(0,1,1,0)^T$ corresponding to the zero eigenvalues. Therefore the condensate at this momentum is a linear combination of these two vectors

$$\langle\Psi_{\mathbf{k}=(0,0)}\rangle=z_1(1,0,0,-1)^T+z_2(0,1,1,0)^T. \tag{21}$$

Complex numbers z_1 and z_2 determine the orientation of staggered moments, as in the case of triangular lattice.[30] Define $z=(z_1,z_2^*)^T$, then the Schwinger bosons on sublattice $u(v)$ becomes $\langle b_\alpha\rangle=z(\langle b_\alpha\rangle=i\sigma^y z^*)$. The moment on sublattice $u(v)$ is $\mathbf{M}_u=(1/2)z^\dagger\boldsymbol{\sigma}z$ $[\mathbf{M}_v=(1/2)z^T(-i\sigma^y)\boldsymbol{\sigma}(i\sigma^y)z^*=-(1/2)z^\dagger\boldsymbol{\sigma}z=-\mathbf{M}_u]$. This is the Néel order.

At $A_2/A_1=1/2$, the minima of dispersion jump to six T points on the Γ$-K(K')$ lines with $|\mathbf{k}|=\pi$ [BZ corner $K(K')$ point has $|\mathbf{k}|=4\pi/3$]. Further increase A_2/A_1 to $+\infty$ will move the minima toward the $K(K')$ points [see Fig. 6(a)]. The boson condensation in this case will in general lead to incommensurate magnetic order. Note that the $A_2/A_1=+\infty$ limit is just two copies of decoupled zero-flux triangular lattice Schwinger boson mean field theory.[24,30]

A mean field phase diagram in terms of the variational parameter A_2/A_1 and average boson density is constructed as Fig. 1. There is a very small parameter range $0.493<A_2/A_1<0.516$ where the critical boson density is greater than unity, namely, the spin-1/2 system will remain to be a gapped spin liquid. This is particularly promising for explaining the numerically observed transition from short-range RVB to Néel state as U/t is increased. Because increasing of U/t will decrease $J_2/J_1\propto(t/U)^2$, and thus decrease A_2/A_1, the spin-1/2 system will move to the left along the dash line in Fig. 1, and cross the mean field phase boundary between the zero-flux Z_2 spin liquid and Néel order.

In this scenario, the spin liquid will be very close to the mean field tricritical point $A_2/A_1=1/2$ and $\langle\hat{n}\rangle_{\mathrm{MF}}\approx 1.18$. Therefore the momenta of low-energy bosons are not only the Γ point but also the six $T(|\mathbf{k}|=\pi)$ points in Fig. 6(a). The dispersion for $A_2/A_1=1/2$ and $\langle\hat{n}\rangle_{\mathrm{MF}}=1$ (spin-1/2) case is drawn along high-symmetry directions in Fig. 5 to illustrate this point. The dynamical spin susceptibility at low frequency around the spin gap will have peaks at wave vectors connecting two (can be the same) boson condensation momenta, these include not only the Γ point but also three Brillouin-zone-edge center M points, and these six T points, and six other D points [Fig. 6(a)].

B. Critical field theory for the transition from zero-flux state to Néel order

Considering the spatial-temporal fluctuations of the would-be boson condensate z in the zero-flux state close to the transition into Néel order, one can derive the critical field theory. The detailed derivation is given in Appendix C. The boson part of the Lagrangian reads

$$\mathcal{L}_z=\int d^2\mathbf{r}\Bigg\{|D_\tau z|^2+c^2|D_{\mathbf{r}}z|^2+m^2|z|^2+\lambda_3 z^*\left[\sum_{j=1}^{3}(\mathbf{e}_j\cdot D_{\mathbf{r}})^3\right]z+\mathrm{c.c.}+\lambda_H\Phi\cdot z^T(i\sigma^y)\left[\sum_{j=1}^{3}(\mathbf{d}_j\cdot D_{\mathbf{r}})^3\right]z+\mathrm{c.c.}\Bigg\}, \tag{22}$$

where τ is the imaginary time, $\mathbf{r}$ is the spatial coordinates, $\Phi\sim A_2$ is the scalar Higgs field, c.c. means complex conjugate of the previous term, and D is the covariant derivative with minimal coupling to the compact U(1) gauge field coming from the Schwinger boson representation. Vectors $\mathbf{e}_1=(2\mathbf{a}_2-\mathbf{a}_1)/3$, $\mathbf{e}_2=-(\mathbf{a}_2+\mathbf{a}_1)/3$, $\mathbf{e}_3=(2\mathbf{a}_1-\mathbf{a}_2)/3$, $\mathbf{d}_1=-\mathbf{a}_1$, $\mathbf{d}_2=\mathbf{a}_2$, and $\mathbf{d}_3=\mathbf{a}_1-\mathbf{a}_2$ are defined for convenience. The velocity c and boson mass m and coupling constants λ_3 and λ_H can, in principle, be derived from the microscopic theory. Magnetic-ordering transition happens when the mass m vanishes.

The transformation rules of z and Φ fields under space-group symmetry can be derived from the zero-flux ($p_1=0$) PSG Eq. (14)

$$T_1,T_2: z \to z, \quad \Phi \to \Phi, \tag{23a}$$

$$C_6: z \to -\sigma^y z^*, \quad \Phi \to \Phi, \tag{23b}$$

$$\sigma: z \to -i\sigma^y z^*, \quad \Phi \to \Phi. \tag{23c}$$

The Higgs field $\Phi \sim A_2$ transforms trivially. The Lagrangian Eq. (22) is invariant under the PSG.

Note that the form of the coupling between bosons z and the Higgs field Φ is constrained by the PSG, namely, the microscopic lattice symmetry. It is very different from the typical coupling[21] which involves only one spatial derivative, such coupling would violate the sixfold rotation symmetry here. Naive power counting shows that this coupling here, with cubic power of spatial derivatives, is irrelevant, which means the Higgs field will dynamically decouple from the bosons at low energy. Considering the anomalous dimensions will not change this conclusion. This is why the Z_2 state here still produces a commensurate Néel order upon boson condensation in contrast to the conventional theory[21] where it usually becomes a noncollinear incommensurate order. However, the Higgs mechanism for reducing U(1) to Z_2 is still intact, as long as the Higgs condensate $\Phi \sim A_2$ is nonzero, providing stability against confinement in compact U(1) gauge theory in 2+1 dimension. It would be very interesting to see if the same critical field theory can be reached from the Néel order side.

At the transition point, the low-energy theory is the O(4) invariant critical theory for the transition between a spiral magnet and a gapped spin liquid.[41–43] The scaling properties have been studied within large-N expansion[41,42] and also numerically.[43] For example, spin-spin correlations will have power-law scaling at large distance

$$\langle \mathbf{S}(0) \cdot \mathbf{S}(\mathbf{r}) \rangle \sim |\mathbf{r}|^{-\eta}, \tag{24}$$

where η has been numerically determined[43] as $\eta = 1.373(3)$. This can be checked with the finite-size scaling results of the Hubbard model when U/t is tuned to the magnetic ordering transition.

C. π-flux State

Now we consider the π-flux state in Fig. 4. The unit cell for the mean field theory is doubled along $\mathbf{a}_2$ direction and contains four sites u,v,p,q. The Brillouin zone is halved as shown in Fig. 6(b). However, we stress here that the physical spin state obtained from imposing the constraint Eq. (4) on this mean field wave function has the original translation symmetry of honeycomb lattice and this is guaranteed by the PSG.

The mean field Hamiltonian after Fourier transform looks like, up to a constant

$$\sum_{\mathbf{k}} \Psi_{\mathbf{k}}^\dagger \begin{pmatrix} \mu \mathbf{1}_{4\times 4} & A_1 P_1 + A_2 P_2 \\ -A_1 P_1 - A_2^* P_2 & \mu \mathbf{1}_{4\times 4} \end{pmatrix} \Psi_{\mathbf{k}}, \tag{25}$$

where $\Psi_{\mathbf{k}}$ is an eight-component field, $\Psi_{\mathbf{k}} = (b_{\mathbf{k}u\uparrow}, b_{\mathbf{k}v\uparrow}, b_{\mathbf{k}p\uparrow}, b_{\mathbf{k}q\uparrow}, b^\dagger_{-\mathbf{k},u\downarrow}, b^\dagger_{-\mathbf{k},v\downarrow}, b^\dagger_{-\mathbf{k},p\downarrow}, b^\dagger_{-\mathbf{k},q\downarrow})^T$, $\mathbf{1}_{4\times 4}$ is 4×4 identity matrix, and $P_{1,2}$ are 4×4 antihermitian matrices

$$P_1 = \frac{1}{2} \begin{pmatrix} 0 & 1 & 0 & -\epsilon_3^{-1} + \epsilon_2 \\ -1 & 0 & -1 - \epsilon_1^{-1} & 0 \\ 0 & 1 + \epsilon_1 & 0 & 1 \\ \epsilon_3 - \epsilon_2^{-1} & 0 & -1 & 0 \end{pmatrix}, \tag{26}$$

$$P_2 = \frac{1}{2} \begin{pmatrix} 2i\sin(k_1) & 0 & 1 - \epsilon_2 - \epsilon_1^{-1} - \epsilon_3^{-1} & 0 \\ 0 & -2i\sin(k_1) & 0 & 1 - \epsilon_2 - \epsilon_1^{-1} - \epsilon_3^{-1} \\ -1 + \epsilon_2^{-1} + \epsilon_1 + \epsilon_3 & 0 & -2i\sin(k_1) & 0 \\ 0 & -1 + \epsilon_2^{-1} + \epsilon_1 + \epsilon_3 & 0 & 2i\sin(k_1) \end{pmatrix} \tag{27}$$

with the short-hand notations $\epsilon_1 = e^{ik_1}$, $\epsilon_2 = e^{-ik_2'}$, $\epsilon_3 = e^{i(k_2' - k_1)}$, and $k_1 \equiv \mathbf{k} \cdot \mathbf{a}_1$, $k_2' \equiv \mathbf{k} \cdot (2\mathbf{a}_2)$. Note that k_2' is twice of the k_2 in previous section.

The mean field Hamiltonian can, in principle, be diagonalized by a Bogoliubov transformation to give the mean field dispersion. However, with A_1 and A_2 both nonzero this is very difficult analytically. In the following we will set A_2 to zero and present some results for the nearest-neighbor ansatz. The mean field dispersion with only nearest-neighbor ansatz has two branches, each is fourfold degenerate

$$E_\pm^{(\pi)}(\mathbf{k}) = \sqrt{\mu^2 - A_1^2 [3/4 \pm \sqrt{f(\mathbf{k})}]}, \tag{28}$$

where $f(\mathbf{k}) = [3 + \cos(2k_1) + \cos(k_2') - \cos(2k_1 - k_2')]/8$.

Average boson density $\kappa \equiv \langle \hat{n} \rangle_{\mathrm{MF}}$ is

$$\kappa = \int \frac{dk_1 dk_2'}{4\pi^2} \frac{1}{2} \left(\frac{|\mu|}{E_+^{(\pi)}(\mathbf{k})} + \frac{|\mu|}{E_-^{(\pi)}(\mathbf{k})} \right) - 1. \tag{29}$$

The critical boson density is achieved when $|\mu/A_1| = \sqrt{3/2}$, and $\kappa_c = 2.14 > 1$. Taken at face value it means this state can remain quantum disordered for spin-1/2 and even spin-1 systems.

The bosons will condense at four momenta in the reduced Brillouin zone [see Fig. 6(b)], which are $\mathbf{k} = \pm \mathbf{k}_{c1} = \pm (k_1 = \pi/6, k_2' = -\pi/3)$ and $\mathbf{k} = \pm \mathbf{k}_{c2} = \pm (k_1 = -5\pi/6, k_2' = -\pi/3)$. The condensate at each momentum will be

$$\langle \Psi_{\mathbf{k}=+(\pi/6,-\pi/3)} \rangle = z_1 V_1 + z_2 V_2, \tag{30a}$$

$$\langle \Psi_{\mathbf{k}=-(\pi/6,-\pi/3)} \rangle = w_1 V_1^* + w_2 V_2^*, \tag{30b}$$

$$\langle \Psi_{\mathbf{k}=+(-5\pi/6,-\pi/3)} \rangle = z_3 V_3 + z_3 V_4, \tag{30c}$$

$$\langle \Psi_{\mathbf{k}=-(-5\pi/6,-\pi/3)} \rangle = w_3 V_3^* + w_4 V_4^* \tag{30d}$$

with complex coefficients $z_{1,2,3,4}, w_{1,2,3,4}$, and the complex vectors V_1, V_2 are eigenvectors of Eq. (25) at $\mathbf{k}_{c1}=(\pi/6, -\pi/3)$ with eigenvalue zero, and V_3, V_4 are for $\mathbf{k}_{c2}=(-5\pi/6, -\pi/3)$. The vectors $V_{1,2,3,4}$ are explicitly given below

$$V_1 = (e^{-i\pi/12}, 0, \sqrt{2+\sqrt{3}}, 0, 0, -e^{-i\pi/12}\sqrt{2+\sqrt{3}}, 0, -1),$$

$$V_2 = (0, e^{-i\pi/12}\sqrt{2+\sqrt{3}}, 0, -1, e^{-i\pi/12}, 0, \sqrt{2+\sqrt{3}}, 0),$$

$$V_3 = (e^{5i\pi/12}\sqrt{2+\sqrt{3}}, 0, 1, 0, 0, -e^{5i\pi/12}, 0, -\sqrt{2+\sqrt{3}}),$$

$$V_4 = (0, e^{5i\pi/12}, 0, \sqrt{2+\sqrt{3}}, e^{5i\pi/12}\sqrt{2+\sqrt{3}}, 0, 1, 0). \tag{31}$$

Note that $z_{1,2,3,4}, w_{1,2,3,4}$ may not be independent because one need to make sure that the number of condensed bosons on every site is the same.[30]

The magnetic order is complicated but will certainly not be the Neel order. Because bosons have to condense at several different momenta otherwise the condensed boson density (size of the magnetic moment) would be nonuniform on the four sublattices. Without knowing the detailed condensate structure we can still determine the possible magnetic Bragg-peak wave vectors, which are the differences between two-boson condensation momenta. These possible magnetic Bragg peaks are $(k_1, k_2) = \pm(\pi/3 + m\pi, -\pi/3 + n\pi), \pm(m\pi, n\pi)$ with integers m, n and are illustrated in Fig. 6(b). These momenta are accessible on 6×6, 12×12, and 18×18 lattices used in the quantum Monte Carlo study.[19] So whether this π-flux state is realized can be tested by measuring static spin structure factor at these momenta in the magnetic ordered phase. The detailed magnetic order pattern will be very nontrivial like that from the triangular lattice π-flux state[24] but will be left for future works.

We will not study the effect of the next-nearest-neighbor coupling A_2 in the π-flux state in this paper. We just note here that with $A_2/A_1 \to \infty$, the mean field ansatz Fig. 4 becomes two copies of decoupled π-flux states on the triangular lattice found in Ref. 24.

It would be interesting to realize this π-flux state in a simple spin model on honeycomb lattice. However, for the nearest-neighbor Heisenberg model general argument[37] indicates that zero-flux state will always have lower energy than the π-flux state. Ring-exchange interaction (for the six sites around a hexagon) may favor the π-flux state.[24] However, the natural sign of the ring-exchange coupling derived from the Hubbard model will actually favor the zero-flux state as discussed in Ref. 24. Thus the π-flux state is not likely realized in the numerical simulation of the Hubbard model.[19]

V. CONCLUSIONS

In hope of understanding the numerical evidence of a short-range RVB state found by recent quantum Monte Carlo simulations of honeycomb lattice Hubbard model,[19] and the possibly continuous quantum phase transition from the short-range RVB to the magnetic ordered Néel state, we studied the Z_2 spin liquids within the Schwinger boson mean field theory. Applying the projective symmetry group method for Schwinger boson states[24] we completely classified possible Z_2 Schwinger boson spin liquid states on honeycomb lattice. Symmetry allowed mean field ansatz are derived for up to fourth neighbor couplings, which can be used for future studies of the Schwinger boson mean field theory. Assuming nonzero nearest-neighbor and next-nearest-neighbor mean field couplings A_1 and A_2, there are only two Z_2 states on honeycomb lattice which do not break any lattice symmetry. The two states are differentiated by the gauge-invariant flux, zero or π, in the elementary hexagon.

The zero-flux state is a very promising candidate for the numerically observed short-range RVB state. Its critical boson density decreases from 1.18 at $A_2/A_1=1/2$ to 0.516 at $A_2/A_1=0$, and a continuous quantum phase transition to Néel order will happen in this process, emulating the behavior of the numerically studied Hubbard model when U/t increase from below $U/t=4.3$ to $+\infty$. The critical field theory for the phase transition to Néel order is an O(4) invariant theory Eq. (22), with an irrelevant coupling between Higgs field and boson fields involving cubic power of spatial derivatives, unlike the conventional form of such coupling with only one spatial derivative.[21] Therefore it allows for a direct transition from a Z_2-gapped spin liquid to a Néel order. In this scenario the spin liquid could have soft spin fluctuations at not only the ordering wave vector Γ point but also at Brillouin-zone-edge center M points, and six $T(|\mathbf{k}|=\pi)$ points, and six other D points [see Fig. 6(a)], which can be checked by numerically calculating the dynamical spin susceptibility. Also the magnetic ordering transition will be an O(4) invariant theory, the (finite-size) scaling of correlation functions can be checked against known results,[41–43] e.g., spin-spin correlation function behaves as $|\mathbf{r}|^{-1.373}$ at large distance $\mathbf{r}$.

The π-flux state has the critical mean field boson density $\kappa_c \approx 2.13$ (with only nearest-neighbor mean field couplings) well above unity. Boson condensation in the π-flux state will lead to magnetic Bragg peak at several wave vectors as show in Fig. 6(b), including the Néel order wave vector, which can be checked in the numerical simulations of the magnetic ordered phase. But for energetic reasons it is not likely realized in the Hubbard model.

There are still many remaining interesting questions and possible future directions in this problem. (1) The Z_2 spin liquid on a torus will have fourfold ground-state degeneracy which was not observed in the numerical simulation.[19] It is possible that ground states in different topological sector actually carry different physical quantum number, e.g., quantum number with respect to sixfold rotation, thus not all of them were accessed in the simulation. It would be useful to work out these vison quantum numbers which can guide the search of topological order in the numerical work. (2) The critical field theory Eq. (22) is derived from the spin liquid

side. It would be very interesting to start from the Néel-ordered side and see if the same conclusion can be reached. For comparison to numerics it may also be useful to compute the scaling properties of other observables. Also the mean field tricritical point in Fig. 1, where bosons condense at Γ and six T points, might also be of some interest. (3) The continuous Mott transition is not easy to understand with the Schwinger boson formalism but is more natural in the fermionic spinon formulation. It may be interesting to study the Z_2 states with fermionic spinons, and see if a unified picture of both continuous Mott transition and magnetic ordering transition can be achieved. (4) It may be useful to derive the effective spin model from the Hubbard model to high orders of t/U, then compute energetics of the zero-flux Z_2 spin liquid state and other possible states, in order to produce a physical (mean field) phase diagram. (5) It may also be useful to have a concrete simple spin model which shows one of these Z_2 spin liquid ground states. J_1-J_2 model may be a good example but unfortunately has sign problem preventing large scale quantum Monte Carlo simulations.

There has been a proposal of nonmagnetic insulator state in honeycomb Hubbard model close to the metal-insulator transition.[44] Its relation to the present study is, however, unclear yet. Also in a recent paper by Xu and Sachdev[45] another Z_2 spin liquid state was proposed through a different formalism. Its relation to the Z_2 spin liquid studied here remains to be clarified.

ACKNOWLEDGMENTS

The author thanks Ying Ran for bringing Ref. 19 to his attention, and acknowledges very helpful discussions with Ying Ran, Todadri Senthil, Ashvin Vishwanath, Xiao-Gang Wen, and Cenke Xu. The author is especially grateful to Todadri Senthil for correcting the interpretation of the continuum-field theory, Eq. (22).

APPENDIX A: ALGEBRAIC SOLUTION OF THE Z_2 PSG ON HONEYCOMB LATTICE

In this appendix we list the detailed steps for solving the Z_2 PSGs on honeycomb lattice. The algebraic solutions will determine all possible symmetric Z_2 states within the Schwinger boson formalism.

The lattice and its space-group generators are described in Sec. III and illustrated in Fig. 2. All independent commutation relations between the space-group generators are

$$\begin{aligned} T_1^{-1}T_2T_1T_2^{-1} &= T_1^{-1}T_2^{-1}T_1T_2 = T_1^{-1}C_6T_1T_2^{-1}C_6^{-1} = T_2^{-1}C_6T_1C_6^{-1} \\ &= C_6^6 = T_1^{-1}\sigma T_1\sigma^{-1} = T_2^{-1}\sigma T_1T_2^{-1}\sigma^{-1} = \sigma^2 \\ &= \sigma C_6\sigma C_6 = \mathbf{1}, \end{aligned} \tag{A1}$$

where 1 is the identity element of the space group.

For reasons discussed in Sec. II we will assume the invariant gauge group is Z_2. The generator of invariant gauge group (IGG) is

$$\hat{b}_{j\alpha} \to -\hat{b}_{j\alpha}, \quad \alpha = \uparrow,\downarrow, \forall \text{ site } j. \tag{A2}$$

For each space-group element X, associate a gauge-group element [U(1) phase] $\exp[i\phi_X(j)]$ such that the mean field Hamiltonian is invariant under the combined PSG operation

$$b_{j\alpha} \to \exp[i\phi_X(j)]b_{X(j)\alpha}. \tag{A3}$$

Note that these phases $\phi_X(j)$ and later equations of these phases should be understood with implicit modulo 2π.

If a gauge transformation $b_{is} \to e^{i\phi(i)}b_{is}$ is applied, then PSG elements transform as Eq. (27) $\phi_X(i) \to \phi_X(i) + \phi(i) - \phi[X^{-1}(i)]$. Using this gauge freedom one can always assume (on open boundary condition)

$$\phi_{T_1}(x,y,w) = 0, \quad \phi_{T_2}(x=0,y,w) = 0, \tag{A4}$$

where $w=u,v$ labels sublattice, (x,y) labels unit cell.

For simplicity of notations we define two forward finite differences $\Delta_1 f(x,y) \equiv f(x+1,y) - f(x,y)$ and $\Delta_2 f(x,y) \equiv f(x,y+1) - f(x,y)$. From $T_1^{-1}T_2T_1T_2^{-1} = \mathbf{1}$, convert each space-group element to its corresponding PSG element, the identity 1 to an unknown IGG element $b_{i\alpha} \to e^{ip_1\pi}b_{i\alpha}$, we have

$$\Delta_1\phi_{T_2}(x,y,w) = p_1\pi \tag{A5}$$

with integer $p_1=0$, 1, mod 2. Later used integers $p_{2,3,4,5,6,7,8,9}$ are also Z_2 integers. And equations between them should be understood with implicit modulo 2. Solution of this equation together with Eq. (A4) is

$$\phi_{T_2}(x,y,w) = p_1\pi x. \tag{A6}$$

From this one can already conclude that the flux in the elementary hexagon is $p_1\pi$.

At this stage there are four remaining gauge freedoms. These gauge transformations do not change ϕ_{T_1}, ϕ_{T_2} up to IGG elements but can be used to simplify other PSG elements.

Gauge freedom I: a global phase rotation, does not change any PSG elements

$$b_{(x,y,w)\alpha} \to e^{i\phi}b_{(x,y,w)\alpha}. \tag{A7}$$

This can be used to fix one of the A_{ij} to be real positive. We will fix $A_{(0,0,u)\to(0,0,v)}$ to be real positive.

Gauge freedom II

$$b_{(x,y,w)\alpha} \to e^{i\pi x}b_{(x,y,w)\alpha}. \tag{A8}$$

Gauge freedom III

$$b_{(x,y,w)\alpha} \to e^{i\pi(x+y)}b_{(x,y,w)\alpha}. \tag{A9}$$

Gauge freedom IV: staggered phase rotation

$$b_{(x,y,u)} \to e^{+i\phi}b_{(x,y,u)}, \quad b_{(x,y,v)} \to e^{-i\phi}b_{(x,y,v)}. \tag{A10}$$

From $T_1^{-1}C_6T_1T_2^{-1}C_6^{-1} = T_2^{-1}C_6T_1C_6^{-1} = \mathbf{1}$ we have

$$\Delta_1\phi_{C_6}(x,y,w) = p_1\pi(x+y) + p_2\pi, \tag{A11a}$$

$$\Delta_2\phi_{C_6}(x,y,w) = p_1\pi x + p_3\pi. \tag{A11b}$$

Its solution is

$$\phi_{C_6}(x,y,w) = \phi_{C_6}(0,0,w) + p_1\pi\frac{x(x+2y-1)}{2} + p_2\pi x + p_3\pi y. \tag{A12}$$

If gauge freedom II is applied, p_3 becomes p_3+1, therefore p_3 can always be assumed as zero. If gauge freedom III is applied, p_2 becomes p_2+1, and $\phi_{C_6}(0,0,v)$ becomes $\phi_{C_6}(0,0,v)+\pi$, therefore p_2 can always be assumed as zero as well. If gauge freedom IV is applied, $\phi_{C_6}(0,0,u)$ becomes $\phi_{C_6}(0,0,u)+\phi$ and $\phi_{C_6}(0,0,v)$ becomes $\phi_{C_6}(0,0,v)-\phi$, therefore $\phi_{C_6}(0,0,u)$ and $\phi_{C_6}(0,0,v)$ can always be assumed as the same. And now we have exhausted all gauge freedoms.

From $T_1^{-1}\sigma T_1\sigma^{-1}=T_2^{-1}\sigma T_1 T_2^{-1}\sigma^{-1}=\mathbf{1}$ we have

$$\Delta_1\phi_\sigma(x,y,w) = p_4\pi, \tag{A13a}$$

$$\Delta_2\phi_\sigma(x,y,w) = p_1\pi y + p_5\pi. \tag{A13b}$$

Its solution is

$$\phi_\sigma(x,y,w) = \phi_\sigma(0,0,w) + p_1\pi y(y-1)/2 + p_4\pi x + p_5\pi y. \tag{A14}$$

From $C_6^6=\mathbf{1}$ we have a constraint on $\phi_{C_6}(0,0,w)$

$$3[\phi_{C_6}(0,0,u) + \phi_{C_6}(0,0,v)] + (p_1+p_2)\pi = p_6\pi. \tag{A15}$$

From $\sigma^2=\mathbf{1}$ we have a constraint on $\phi_\sigma(0,0,w)$

$$\phi_\sigma(0,0,u) + \phi_\sigma(0,0,v) + \pi(p_1y^2 + p_4y) = p_7\pi. \tag{A16}$$

This ensures $p_4=p_1 \bmod 2$ because this equation is true for all y.

From $\sigma C_6\sigma C_6=\mathbf{1}$ we have a constraint on $\phi_{C_6}(0,0,w)$ and $\phi_\sigma(0,0,w)$

$$2\phi_\sigma(0,0,v) + 2\phi_{C_6}(0,0,u) = 2\phi_\sigma(0,0,u) + 2\phi_{C_6}(0,0,v) = p_8\pi. \tag{A17}$$

Therefore we have

$$\phi_\sigma(0,0,u) - \phi_\sigma(0,0,v) = p_9\pi. \tag{A18}$$

And the solution of $\phi_{C_6}(0,0,w)$ and $\phi_\sigma(0,0,w)$ is

$$\phi_\sigma(0,0,u) = (p_7+p_9)\pi/2 \bmod 2\pi, \tag{A19}$$

$$\phi_\sigma(0,0,v) = (p_7-p_9)\pi/2 \bmod 2\pi, \tag{A20}$$

$$\phi_{C_6}(0,0,w) = (p_7+p_8+p_9)\pi/2 \bmod 2\pi \tag{A21}$$

and $p_1+p_6+p_7+p_8+p_9=0 \bmod 2$ thus p_6 can be eliminated.

Considering all these constraints, $p_2=p_3=0$, $p_4=p_1$, and $p_6=p_1+p_7+p_8+p_9$, we will reach the final solution of PSG shown in the main text Eq. (13) with only five free Z_2 integer parameters p_1,p_5,p_7,p_8,p_9.

APPENDIX B: REALIZATIONS OF THE Z_2 PSG ON HONEYCOMB LATTICE: MEAN FIELD ANSATZ

In this appendix we will use the solution of PSG to construct symmetry allowed mean field ansatz. We will list the PSG allowed ansatz up to fourth neighbors of the honeycomb lattice.

The algebraic solution of PSG is very general and usually contains many free parameters. When realized by a particular kind of ansatz, e.g., nearest-neighbor ansatz, the number of free parameter will be greatly reduced because there will be further constraints on the PSG. For example, if A_{ij} is nonzero, and there is a nonidentity space-group element X such that $X(i)=j$, $X(j)=i$, namely, the bond ij maps to its inverse ji, then $A_{ji}=-A_{ij}=\exp[i\phi_X(j)+i\phi_X(i)]A_{ij}$, therefore $\phi_X(j)+\phi_X(i)=\pi \bmod 2\pi$. All such independent nonidentity space-group elements X, which map ij to itself or its inverse, need to be checked. The ansatz A_{ij} is compatible with this PSG if all such checks are passed. Then ansatz on all symmetry related bonds can be generated by applying the PSG operations.

Nearest-neighbor ansatz $A_{\langle ij\rangle}$: assume $A_{(0,0,u)\to(0,0,v)}=A_1>0$. This bond under σ becomes its inverse $(0,0,v)\to(0,0,u)$, then $\phi_\sigma(0,0,u)+\phi_\sigma(0,0,v)=\pi$, therefore $p_7=1$. This bond under $T_1^{-1}C_6^3$ becomes its inverse as well, then $\phi_{C_6}(0,0,u)+2\phi_{C_6}(1,-1,v)+2\phi_{C_6}(1,0,u)+\phi_{C_6}(1,0,v)=\pi$, therefore $p_7+p_8+p_9=1$. Also under $C_6\sigma C_6$ it becomes its inverse, then $\phi_{C_6}(1,-1,v)+\phi_{C_6}(0,0,u)+\phi_\sigma(0,1,u)+\phi_\sigma(0,0,v)+\phi_{C_6}(0,0,v)+\phi_{C_6}(0,0,u)=\pi$, therefore $p_1+p_5+p_7=1$. These constraints require $p_5=p_1$, $p_7=1$, and $p_8=p_9 \bmod 2$.

All nearest-neighbor ansatz on the lattice are

$$A_{(x,y,u)\to(x,y,v)} = +A_1, \tag{B1a}$$

$$A_{(x,y,u)\to(x+1,y-1,v)} = +(-1)^{p_1y}(-1)^{p_1}A_1, \tag{B1b}$$

$$A_{(x,y,u)\to(x,y-1,v)} = +A_1. \tag{B1c}$$

Next-nearest-neighbor ansatz $A_{\langle\langle ij\rangle\rangle}$: assume second neighbor $A_{(0,0,u)-(0,1,u)}$ is nonzero A_2. This bond under σC_6 becomes its inverse, then $\phi_\sigma(0,0,u)+\phi_\sigma(0,1,u)+\phi_{C_6}(1,-1,v)+\phi_{C_6}(0,0,v)=\pi$, therefore $p_1+p_5+p_8=1$. Combined with constraints from nonzero nearest-neighbor ansatz, this gives $p_5=p_1$, $p_7=p_8=p_9=1$. So there is only one free Z_2 integer p_1.

All next-nearest-neighbor ansatz on the lattice are

$$A_{(x,y,u)\to(x,y+1,u)} = +A_2, \tag{B2a}$$

$$A_{(x,y,v)\to(x+1,y,v)} = -(-1)^{p_1y}A_2, \tag{B2b}$$

$$A_{(x,y+1,u)\to(x+1,y,u)} = +(-1)^{p_1y}A_2, \tag{B2c}$$

$$A_{(x+1,y,v)\to(x+1,y-1,v)} = -A_2, \tag{B2d}$$

$$A_{(x+1,y,u)\to(x,y,u)} = +(-1)^{p_1y}(-1)^{p_1}A_2, \tag{B2e}$$

$$A_{(x+1,y-1,v)\to(x,y,v)} = -(-1)^{p_1y}(-1)^{p_1}A_2. \tag{B2f}$$

With both nearest- and next-nearest-neighbor ansatz nonzero, there are only one free Z_2 integer $p_1=0,1$ in the PSG solution so there are only two different Schwinger mean field theories. The ansatz are pictorially shown in Figs. 3 and 4.

They are named as the zero-flux ($p_1=0$) and π- flux ($p_1=1$) states for their different gauge-invariant flux in a hexagon.

Third neighbor ansatz: assume third neighbor $A_{(1,-1,v)-(0,1,u)}$ is nonzero A_3. This bond under σ becomes its inverse, then $\phi_\sigma(1,-1,v)+\phi_\sigma(0,1,u)=\pi$, therefore $p_7=1$. Also under C_6^3 it becomes its inverse, then $\phi_{C_6}(1,0,u)+\phi_{C_6}(0,0,v)+\phi_{C_6}(1,0,v)+\phi_{C_6}(0,0,u)+\phi_{C_6}(1,-1,v)+\phi_{C_6}(0,1,u)=\pi$, therefore $p_1+p_7+p_8+p_9=1$. Then A_3 can be nonzero only in the zero-flux state ($p_1=0$).

In the zero-flux state, all third neighbor ansatz on the lattice are

$$A_{(x+1,y-1,v)\to(x,y+1,u)} = +A_3, \tag{B3a}$$

$$A_{(x+1,y,v)\to(x,y,u)} = +A_3, \tag{B3b}$$

$$A_{(x,y,v)\to(x+1,y,u)} = +A_3. \tag{B3c}$$

Fourth neighbor ansatz: assume fourth neighbor $A_{(0,0,v)\to(1,1,u)}$ is nonzero A_4. This bond under $T_2C_6^3$ becomes its inverse, then

$$\begin{aligned}&\phi_{C_6}(0,0,u)+\phi_{C_6}(0,1,v)+\phi_{C_6}(1,-1,v)+\phi_{C_6}(-1,1,u)\\&\quad+\phi_{C_6}(1,0,u)+\phi_{C_6}(0,-1,v)+\phi_{T_2}(1,1,u)+\phi_{T_2}(0,0,v)\\&\quad=\pi,\end{aligned}$$

therefore $p_7+p_8+p_9=1$. This constraint is already required by nonzero nearest-neighbor ansatz.

All fourth neighbor ansatz on the lattice are

$$A_{(x,y,v)\to(x+1,y+1,u)} = +(-1)^{p_1 y}A_4, \tag{B4a}$$

$$A_{(x,y,v)\to(x,y-1,u)} = +A_4, \tag{B4b}$$

$$A_{(x,y,v)\to(x-2,y+2,u)} = +(-1)^{p_1}A_4, \tag{B4c}$$

$$A_{(x,y,v)\to(x-2,y+1,u)} = +(-1)^{p_1}A_4, \tag{B4d}$$

$$A_{(x,y,v)\to(x,y+2,u)} = +A_4, \tag{B4e}$$

$$A_{(x,y,v)\to(x+1,y-1,u)} = +(-1)^{p_1 y}A_4. \tag{B4f}$$

The PSG will also impose constraints on the B_{ij} terms in Eq. (7). For an example, we consider nearest-neighbor $B_{\langle ij\rangle}$. Assume $B_{(0,0,u)\to(0,0,v)}$ is nonzero B_1. This bond under σ becomes its inverse $(0,0,v)\to(0,0,u)$, then $\exp\{i[\phi_\sigma(0,0,v)-\phi_\sigma(0,0,u)]\}B_1=(-1)^{p_9}B_1=-B_1=B_1^*$, therefore the argument $\mathrm{Arg}(B_1^*/B_1)=\pi \bmod 2\pi$. This bond under $T_1^{-1}C_6^3$ becomes its inverse as well, then

$$\begin{aligned}&\phi_{C_6}(1,-1,v)-\phi_{C_6}(0,0,u)+\phi_{C_6}(1,0,u)-\phi_{C_6}(1,-1,v)\\&\quad+\phi_{C_6}(1,0,v)-\phi_{C_6}(1,0,u)=0=\mathrm{Arg}(B_1^*/B_1).\end{aligned}$$

Also under $C_6\sigma C_6$ it becomes its inverse, then

$$\begin{aligned}&\phi_{C_6}(1,-1,v)-\phi_{C_6}(0,0,u)+\phi_\sigma(0,1,u)-\phi_\sigma(0,0,v)\\&\quad+\phi_{C_6}(0,0,v)-\phi_{C_6}(0,0,u)=0=\mathrm{Arg}(B_1^*/B_1).\end{aligned}$$

These conditions imply that B_1 must be zero.

Also consider next-nearest-neighbor $B_{\langle\langle ij\rangle\rangle}$. Assume next-nearest-neighbor $B_{(0,0,u)-(0,1,u)}$ is nonzero B_2. This bond under σC_6 becomes its inverse, then

$$\begin{aligned}&\phi_{C_6}(1,-1,v)-\phi_{C_6}(0,0,v)+\phi_\sigma(0,1,u)-\phi_\sigma(0,0,u)=0\\&\quad=\mathrm{Arg}(B_2^*/B_2),\end{aligned}$$

therefore B_2 must be real.

All next-nearest-neighbor $B_{\langle\langle ij\rangle\rangle}$ are

$$B_{(x,y,u)\to(x,y+1,u)} = +B_2, \tag{B5a}$$

$$B_{(x,y,v)\to(x+1,y,v)} = +(-1)^{p_1 y}B_2, \tag{B5b}$$

$$B_{(x,y+1,u)\to(x+1,y,u)} = +(-1)^{p_1 y}B_2, \tag{B5c}$$

$$B_{(x+1,y,v)\to(x+1,y-1,v)} = +B_2, \tag{B5d}$$

$$B_{(x+1,y,u)\to(x,y,u)} = +(-1)^{p_1 y}(-1)^{p_1}B_2, \tag{B5e}$$

$$B_{(x+1,y-1,v)\to(x,y,v)} = +(-1)^{p_1 y}(-1)^{p_1}B_2. \tag{B5f}$$

APPENDIX C: DERIVATION OF THE CONTINUUM-FIELD THEORY FOR THE TRANSITION FROM ZERO-FLUX Z_2 SPIN LIQUID TO NÉEL ORDER

In this appendix we follow the prescription of Sachdev[40] to derive the continuum-field theory from the zero-flux Schwinger boson mean field Hamiltonian Eq. (16) close to the transition to Néel order. The notations are slightly different from Ref. 40. And for simplicity we omit the compact U(1) gauge field in the derivation, which can be added in the final result by promoting the spatial-temporal derivatives to covariant derivatives.

Rewrite the bosons in terms of the would-be condensate modes ψ at the condensation momentum $\mathbf{k}=0$

$$\begin{aligned}b_{(x,y,u)\alpha} &= \psi_{u\alpha}(x\mathbf{a}_1+y\mathbf{a}_2),\\ b_{(x,y,v)\alpha} &= i\sum_\beta \sigma^y_{\alpha\beta}\psi^*_{v\beta}(x\mathbf{a}_1+y\mathbf{a}_2+\mathbf{e}_1),\end{aligned} \tag{C1}$$

where $\mathbf{e}_1=(2\mathbf{a}_2-\mathbf{a}_1)/3$ is the displacement of v site relative to the u site in the same unit cell.

A gradient expansion is then performed on the real-space terms in the mean field Hamiltonian Eq. (7). The bipartite mean field couplings become, up to cubic power of spatial derivatives (sum over spin indices α,β is implicitly assumed)

$$b_{(x,y,u)\uparrow}b_{(x',y',v)\downarrow} - b_{(x,y,u)\downarrow}b_{(x',y',v)\uparrow} = -\psi_{u\alpha}\left[1 + \Delta\mathbf{r}\cdot\partial_{\mathbf{r}} + \frac{(\Delta\mathbf{r}\cdot\partial_{\mathbf{r}})^2}{2} + \frac{(\Delta\mathbf{r}\cdot\partial_{\mathbf{r}})^3}{6}\right]\psi^*_{v\alpha}(\mathbf{r}), \tag{C2}$$

where $\Delta\mathbf{r}=(x'\mathbf{a}_1+y'\mathbf{a}_2+\mathbf{e}_1)-(x\mathbf{a}_1+y\mathbf{a}_2)$. The nonbipartite mean field couplings are

$$b_{(x,y,u)\uparrow}b_{(x',y',u)\downarrow} - b_{(x,y,u)\downarrow}b_{(x',y',u)\uparrow} = i\sigma^y_{\alpha\beta}\psi_{u\alpha}\left[\Delta\mathbf{r}\cdot\partial_{\mathbf{r}} + \frac{(\Delta\mathbf{r}\cdot\partial_{\mathbf{r}})^2}{2} + \frac{(\Delta\mathbf{r}\cdot\partial_{\mathbf{r}})^3}{6}\right]\psi_{u\beta} \tag{C3}$$

and

$$b_{(x,y,v)\uparrow}b_{(x',y',v)\downarrow} - b_{(x,y,v)\downarrow}b_{(x',y',v)\uparrow} = i\sigma^y_{\alpha\beta}\psi^*_{v\alpha}\left[\Delta\mathbf{r}\cdot\partial_{\mathbf{r}} + \frac{(\Delta\mathbf{r}\cdot\partial_{\mathbf{r}})^2}{2} + \frac{(\Delta\mathbf{r}\cdot\partial_{\mathbf{r}})^3}{6}\right]\psi^*_{v\beta}, \tag{C4}$$

where $\Delta\mathbf{r}=(x'\mathbf{a}_1+y'\mathbf{a}_2)-(x\mathbf{a}_1+y\mathbf{a}_2)$.

Plug these relations into Eq. (7) and use the zero-flux ansatz Fig. 3 with nearest-neighbor and next-nearest-neighbor couplings $A_1>0$ and A_2. After collecting terms up to cubic power of spatial derivatives, the continuum limit Lagrangian $\mathcal{L}$ becomes

$$\begin{aligned}\mathcal{L} = \int \frac{d^2\mathbf{r}}{\sqrt{3}a^2/2}\Bigg\{ & \psi^*_{u\alpha}\frac{d}{d\tau}\psi_{u\alpha} - \psi^*_{v\alpha}\frac{d}{d\tau}\psi_{v\alpha} + \mu(\psi^*_{u\alpha}\psi_{u\alpha} \\ & + \psi^*_{v\alpha}\psi_{v\alpha}) + A_1\psi_{u\alpha}\left[\frac{3}{2} + \frac{\sum_{j=1}^{3}(\mathbf{e}_j\cdot\partial_{\mathbf{r}})^2}{4} + \frac{\sum_{j=1}^{3}(\mathbf{e}_j\cdot\partial_{\mathbf{r}})^3}{12}\right]\psi^*_{v\alpha} \\ & + \text{c.c.} + A_2(1/6)i\sigma^y_{\alpha\beta}\psi_{u\alpha}\left[\sum_{j=1}^{3}(\mathbf{d}_j\cdot\partial_{\mathbf{r}})^3\right]\psi_{u\beta} + \text{c.c.} \\ & + A_2(1/6)i\sigma^y_{\alpha\beta}\psi^*_{v\alpha}\left[\sum_{j=1}^{3}(\mathbf{d}_j\cdot\partial_{\mathbf{r}})^3\right]\psi^*_{v\beta} + \text{c.c.}\Bigg\},\end{aligned} \tag{C5}$$

where c.c. means complex conjugate of the previous term, $\sqrt{3}a^2/2$ is the area of honeycomb unit cell, $a=|\mathbf{a}_1|$ is the lattice constant; $\mathbf{e}_{1,2,3}$ are the three vectors connecting a u site to its nearest-neighbor v sites

$$\mathbf{e}_1=(2\mathbf{a}_2-\mathbf{a}_1)/3, \quad \mathbf{e}_2=-(\mathbf{a}_2+\mathbf{a}_1)/3, \quad \mathbf{e}_3=(2\mathbf{a}_1-\mathbf{a}_2)/3 \tag{C6}$$

and we also define for convenience

$$\mathbf{d}_1=-\mathbf{a}_1, \quad \mathbf{d}_2=\mathbf{a}_2, \quad \mathbf{d}_3=\mathbf{a}_1-\mathbf{a}_2. \tag{C7}$$

Note that many terms are canceled due to the geometry, especially the first derivative terms from the A_2 term cancel because $\Sigma_{j=1}^{3}(\mathbf{d}_j\cdot\partial_{\mathbf{r}})=0$.

Define two fields z and Π from linear combinations of ψ_u and ψ_v

$$z_\alpha=(\psi_{u\alpha}+\psi_{v\alpha})/2, \quad \Pi_\alpha=(\psi_{u\alpha}-\psi_{v\alpha})/2. \tag{C8}$$

Plug this into Eq. (C5), the Lagrangian becomes (spin indices α,β are omitted)

$$\begin{aligned}\mathcal{L} = \int \frac{d^2\mathbf{r}}{\sqrt{3}a^2/2}\Bigg\{ & 2z^*\frac{d}{d\tau}\Pi + 2\Pi^*\frac{d}{d\tau}z + (2\mu - 3A_1)z^*z + (2\mu \\ & + 3A_1)\Pi^*\Pi + a^2(A_1/3)\partial_{\mathbf{r}}z^*\cdot\partial_{\mathbf{r}}z + \text{c.c.} \\ & + (A_1/12)z^*\left[\sum_{j=1}^{3}(\mathbf{e}_j\cdot\partial_{\mathbf{r}})^3\right]z + \text{c.c.} + (A_2/3)z^T(i\sigma^y) \\ & \times\left[\sum_{j=1}^{3}(\mathbf{d}_j\cdot\partial_{\mathbf{r}})^3\right]z + \text{c.c.}\end{aligned} \tag{C9}$$

Note that terms involving both field Π and spatial derivatives are omitted, as they will generate terms in the effective Lagrangian of z with fourth or higher power of spatial derivatives, and the following identity has been used

$$\sum_{i=1}^{3}(\mathbf{e}_i\cdot\partial_{\mathbf{r}})^2 = (2/3)a^2\partial^2_{\mathbf{r}}. \tag{C10}$$

Integrate out the field Π with large gap $2\mu+3A_1$, we get the effective Lagrangian for z

$$\begin{aligned}\mathcal{L}_z = \int d^2\mathbf{r}\Bigg[& \frac{8}{(2\mu+3A_1)\sqrt{3}a^2}\partial_\tau z^*\cdot\partial_\tau z + \frac{2A_1}{3\sqrt{3}}\partial_{\mathbf{r}}z^*\cdot\partial_{\mathbf{r}}z \\ & + \frac{2(2\mu-3A_1)}{\sqrt{3}a^2}z^*z + \frac{A_1}{6\sqrt{3}a^2}z^*\left[\sum_{j=1}^{3}(\mathbf{e}_j\cdot\partial_{\mathbf{r}})^3\right]z + \text{c.c.} \\ & + \frac{2A_2}{3\sqrt{3}a^2}z^T(i\sigma^y)\left[\sum_{j=1}^{3}(\mathbf{d}_j\cdot\partial_{\mathbf{r}})^3\right]z + \text{c.c.}\Bigg].\end{aligned} \tag{C11}$$

The critical point is $A_1/\mu=2/3$ consistent with the mean field solution. The critical boson velocity is proportional to A_1. After a proper rescaling of τ the Lagrangian can be cast into the simple form of Eq. (22). Note that A_2 plays the role of the Higgs field.

[1] P. W. Anderson, Mater. Res. Bull. **8**, 153 (1973).
[2] P. Fazekas and P. W. Anderson, Philos. Mag. **30**, 423 (1974).
[3] R. Coldea, D. A. Tennant, and Z. Tylczynski, Phys. Rev. B **68**, 134424 (2003).
[4] Y. Shimizu, K. Miyagawa, K. Kanoda, M. Maesato, and G. Saito, Phys. Rev. Lett. **91**, 107001 (2003).
[5] J. S. Helton, K. Matan, M. P. Shores, E. A. Nytko, B. M. Bartlett, Y. Yoshida, Y. Takano, A. Suslov, Y. Qiu, J.-H. Chung, D. G. Nocera, and Y. S. Lee, Phys. Rev. Lett. **98**, 107204 (2007).
[6] J. T. Chayes, L. Chayes, and S. A. Kivelson, Commun. Math. Phys. **123**, 53 (1989).
[7] C. D. Batista and S. A. Trugman, Phys. Rev. Lett. **93**, 217202 (2004).
[8] K. S. Raman, R. Moessner, and S. L. Sondhi, Phys. Rev. B **72**, 064413 (2005).
[9] D. F. Schroeter, E. Kapit, R. Thomale, and M. Greiter, Phys. Rev. Lett. **99**, 097202 (2007).
[10] J. D. Reger and A. P. Young, Phys. Rev. B **37**, 5978 (1988).
[11] J. D. Reger, J. A. Riera, and A. P. Young, J. Phys.: Condens. Matter **1**, 1855 (1989).
[12] P. W. Anderson, Phys. Rev. **86**, 694 (1952).
[13] D. A. Huse and V. Elser, Phys. Rev. Lett. **60**, 2531 (1988).
[14] D. A. Huse, Phys. Rev. B **37**, 2380 (1988).
[15] R. R. P. Singh, Phys. Rev. B **39**, 9760 (1989).
[16] Zheng Weihong, J. Oitmaa, and C. J. Hamer, Phys. Rev. B **44**, 11869 (1991).
[17] Zheng Weihong, J. Oitmaa, and C. J. Hamer, Phys. Rev. B **43**, 8321 (1991); J. Oitmaa, C. J. Hamer, and Zheng Weihong, *ibid.* **45**, 9834 (1992).
[18] Z. Noorbakhsh, F. Shahbazi, S. A. Jafari, and G. Baskaran, J. Phys. Soc. Jpn. **78**, 054701 (2009).
[19] Z. Meng, T. Lang, S. Wessel, F. Assaad, and A. Muramatsu, Nature (London) **464**, 847 (2010).
[20] M. Hermele, Phys. Rev. B **76**, 035125 (2007).
[21] S. Sachdev and N. Read, Int. J. Mod. Phys. B **5**, 219 (1991).
[22] I. F. Herbut, B. H. Seradjeh, S. Sachdev, and G. Murthy, Phys. Rev. B **68**, 195110 (2003).
[23] A. H. MacDonald, S. M. Girvin, and D. Yoshioka, Phys. Rev. B **37**, 9753 (1988); **41**, 2565 (1990).
[24] F. Wang and A. Vishwanath, Phys. Rev. B **74**, 174423 (2006).
[25] D. P. Arovas and A. Auerbach, Phys. Rev. B **38**, 316 (1988).
[26] N. Read and S. Sachdev, Phys. Rev. Lett. **66**, 1773 (1991).
[27] X. G. Wen, Phys. Rev. B **44**, 2664 (1991).
[28] M. A. Levin and X.-G. Wen, Phys. Rev. B **71**, 045110 (2005).
[29] R. Moessner, S. L. Sondhi, and E. Fradkin, Phys. Rev. B **65**, 024504 (2001).
[30] S. Sachdev, Phys. Rev. B **45**, 12377 (1992).
[31] C. J. Gazza and H. A. Ceccatto, J. Phys.: Condens. Matter **5**, L135 (1993).
[32] K. Lefmann and P. Hedegård, Phys. Rev. B **50**, 1074 (1994).
[33] G. Misguich, B. Bernu, and C. Lhuillier, J. Low Temp. Phys. **110**, 327 (1998).
[34] R. Flint and P. Coleman, Phys. Rev. B **79**, 014424 (2009).
[35] X.-G. Wen, Phys. Rev. B **65**, 165113 (2002).
[36] Y. Zhou and X. Wen, arXiv:cond-mat/0210662 (unpublished).
[37] O. Tchernyshyov, R. Moessner, and S. L. Sondhi, Europhys. Lett. **73**, 278 (2006).
[38] A. Mattsson, P. Fröjdh, and T. Einarsson, Phys. Rev. B **49**, 3997 (1994).
[39] D. Cabra, C. Lamas, and H. Rosales, arXiv:1003.3226 (unpublished).
[40] S. Sachdev, arXiv:1002.3823 (unpublished).
[41] A. V. Chubukov, T. Senthil, and S. Sachdev, Phys. Rev. Lett. **72**, 2089 (1994).
[42] A. V. Chubukov, S. Sachdev, and T. Senthil, Nucl. Phys. B **426**, 601 (1994).
[43] S. V. Isakov, T. Senthil, and Y. B. Kim, Phys. Rev. B **72**, 174417 (2005).
[44] G. Sun and S. Kou, arXiv:0911.3002 (unpublished).
[45] C. Xu and S. Sachdev, arXiv:1004.5431 (unpublished).